

Solitonlike solutions of magnetostatic equilibria: Plane-symmetric case

Hirotaaka Yoshino

*Department of Physics, University of Alberta,
Edmonton, Alberta, Canada T6G 2G7*

Kohei Onda

*Department of Physics, Graduate School of Science,
Nagoya University, Chikusa, Nagoya 464-8602, Japan*

(Dated: May 28, 2008)

Abstract

We present the plane-symmetric solitonlike solutions of magnetostatic equilibria by solving the nonlinear Grad-Shafranov (GS) equation numerically. The solutions have solitonlike and periodic structures in the x and y directions, respectively, and z is the direction of plane symmetry. Although such solutions are unstable against the numerical iteration, we give the procedure to realize the sufficient convergence. Our result provides the definite answer for the existence of the solitonlike solutions that was questioned in recent years. The method developed in this paper will make it possible to study the axisymmetric solitonlike solutions of the nonlinear GS equation, which could model astrophysical jets with knotty structures.

PACS numbers: 52.35.Sb, 52.30.Cv, 95.30.Qd

I. INTRODUCTION

The magnetostatic equilibria are of fundamental interest, since they well approximate slowly varying magnetically confined plasma configurations. In systems with the helical symmetry (i.e. unification of plane symmetry and axisymmetry), the magnetostatic equilibria are described by the so-called Grad-Shafranov (GS) equation (see [1] for a review). The GS equation is an elliptic equation for the flux function Ψ with a source term depending on two functions of Ψ that can be chosen freely. The solutions of the GS equation are often used in theoretical studies in the contexts of the astrophysics or the tokamak physics.

Recently, the existence of an interesting solution of the GS equation was suggested by Lapenta [2]. In that paper, the GS equation with a cubic source term (say, the cubic GS equation) in the plane-symmetric case was discussed. An analogy between this equation and the cubic Schrödinger equation was pointed out, and the real part of the solution of the cubic Schrödinger equation was presented as an analytic “solution” to the GS equation. This “solution” is periodic in the y direction, and has a solitonlike structure in the x direction. Here, z is the direction of the plane-symmetry. Unfortunately, an erroneous assumption in this analysis was pointed out [3] and thus the “solution” of [2] cannot be accepted. However, Lapenta performed a numerical simulation adopting his “solution” as the initial state and observed that the system is relaxed to a quasi-equilibrium state which maintains the solitonlike structure [4] (until the instability becomes relevant). Then, he claimed that the solitonlike solution has practical applicability and relevance. The discussion that supports the existence of the solitonlike solution was given in [5]. The growth of the instability of the solitonlike structure of this system was simulated in order to discuss the collimation and expansion of astrophysical jets [6].

In this paper, we present the plane-symmetric solitonlike solutions of the cubic GS equation by performing highly accurate numerical calculations. There are several reasons for doing so. First, the question on the existence of the solitonlike solutions of the GS equation should be answered. Although the simulations in [4, 6] strongly indicate the existence of the solitonlike solutions and explain the gross features of such solutions, strictly speaking, the obtained quasi-equilibrium states are not the solutions of the GS equation since they weakly depend on time. Besides, even if we ignore the time dependence, the GS equations which the obtained quasi-equilibrium states satisfy are not necessarily the cubic GS equation, i.e.,

the form of the source term should be different in general. Since the possible existence of the solitonlike solutions attracts attentions, it is worth studying these solutions by directly solving the cubic GS equation.

Second, the numerical technique for solving the nonlinear GS equation should be developed. As we will see later, there is a difficulty in solving the cubic GS equation such that the nontrivial solution of this equation is unstable against the numerical iteration, i.e. the standard technique to solve elliptic partial differential equations. The development of such a technique is important not only in the plane-symmetric case but also in the axisymmetric case, because the solitonlike solution of the axisymmetric GS equation is expected to have interesting astrophysical applications. In fact, the observations of active galactic nuclei (AGN) suggest that the astrophysical jets have the magnetic multiple islands [7]. Several models for such knotty jets have been proposed, and one possible direction is to model the knotty jets as the magnetostatic equilibria in the comoving frames [2, 4, 6, 8, 9]. As the first step to study the axisymmetric nonlinear GS equation, it is useful to begin with the simpler plane-symmetric case where the existence of solitonlike solutions is highly likely. In this paper, we give a procedure to realize the sufficient convergence and successfully obtain the numerically unstable solutions. Here, it has to be mentioned that some isolated axisymmetric toroidal Alfvén solitons were numerically obtained in [10, 11] by combining Fourier transformation and the method of the Green’s function. Although their method can be applicable also for the present cases, our method is somewhat simpler and easier.

This paper is organized as follows. In the next section, we briefly review the GS equation and introduce the cubic GS equation. The asymptotic behavior of the solitonlike solution is also studied. In Sec. III, we explain the numerical method and estimate the numerical errors. In Sec. IV, the numerical results are presented. Some properties of the obtained solution are also examined. Sec. V is devoted to summary and discussion. In this paper, we adopt the unit where the vacuum permeability $\mu = 1$ because it can be restored by dimensional considerations if necessary.

II. THE GRAD-SHAFRANOV EQUATION

In this section, we review the Grad-Shafranov (GS) equation for the plane-symmetric case and introduce the assumption on the arbitrary functions that leads to the cubic GS

equation. Then we explain our requirements on the behavior of the solution.

We consider static configurations where the magnetic fields \mathbf{B} are embedded in an ideal plasma with velocity $\mathbf{v} = 0$. The basic equations are Ampere's law and the force balance equation:

$$\mathbf{J} = \nabla \times \mathbf{B}, \quad (1)$$

$$\mathbf{J} \times \mathbf{B} = \nabla p, \quad (2)$$

with the Gauss law $\nabla \cdot \mathbf{B} = 0$. Here, \mathbf{J} is the electric current and p is the pressure of the plasma. Note that in the static configurations, the condition of magnetic confinement $\mathbf{E} = -\mathbf{v} \times \mathbf{B}$ just indicates the absence of the electric fields.

We introduce the Cartesian coordinates (x, y, z) and assume the plane-symmetry in the z direction. Then, the magnetic field can be given by

$$\mathbf{B} = \mathbf{e}_z \times \nabla \Psi(x, y) + B_z(x, y)\mathbf{e}_z, \quad (3)$$

where $\Psi(x, y)$ is the so-called flux function and \mathbf{e}_z is the unit vector in the z direction. This formula satisfies the Gauss law automatically. By Ampere's law (1), the electric current is calculated as

$$\mathbf{J} = (\nabla^2 \Psi)\mathbf{e}_z + (\nabla B_z) \times \mathbf{e}_z. \quad (4)$$

Substituting this formula into Eq. (2), we find

$$[(\nabla \Psi \times \nabla B_z) \cdot \mathbf{e}_z]\mathbf{e}_z = \nabla p + (\nabla^2 \Psi)\nabla \Psi + B_z \nabla B_z. \quad (5)$$

Since the left hand side is the vector in the z direction while the right hand side is the vector in the (x, y) -plane, both sides have to be zero:

$$(\nabla \Psi \times \nabla B_z) \cdot \mathbf{e}_z = 0; \quad (6)$$

$$\nabla p + (\nabla^2 \Psi)\nabla \Psi + B_z \nabla B_z = 0. \quad (7)$$

Eq. (6) indicates $\nabla \Psi \parallel \nabla B_z$, and then Eq. (7) indicates $\nabla \Psi \parallel \nabla p$. Therefore, the contours of B_z , p , and Ψ should coincide, and at least locally B_z and p are given by

$$B_z = f(\Psi), \quad p = g(\Psi), \quad (8)$$

where f and g can be chosen arbitrarily as long as they are regular and $g' > 0$. Then, Eq. (7) is rewritten as

$$\nabla^2 \Psi = -g' - ff'. \quad (9)$$

This is the GS equation for the plane-symmetric case.

In this paper, we consider the situations where the GS equation (9) is reduced to the following form:

$$\nabla^2\Psi = -\Psi (\alpha_0^2 + \beta_0^2\Psi^2). \quad (10)$$

Here, α_0 and β_0 are assumed to be positive without loss of generality. Since the source term has the cubic term, we call this equation the cubic GS equation. Eq. (10) can be derived if we choose the functions f and g satisfying the relation

$$f^2 + 2g = \alpha_0^2\Psi^2 + \frac{1}{2}\beta_0^2\Psi^4 + C. \quad (11)$$

Here, C is a non-negative constant and it is zero if all physical quantities \mathbf{B} and p decay at the distant region. There are infinitely possible choices for f and g , since if $f = f_0$ and $g = g_0$ satisfy Eq. (11), $f = f_0 + \chi$ and $g = g_0 - f_0\chi - \chi^2/2$ also satisfy this relation, where $\chi = \chi(\Psi)$ is an arbitrary function. Therefore, one solution Ψ of the GS equation (10) can describe many different configurations.

It is possible to eliminate α_0 and β_0 from Eq. (10) by introducing the new coordinates

$$\bar{x} := \alpha_0 x, \quad \bar{y} := \alpha_0 y \quad (12)$$

and the rescaled function

$$u := \frac{\beta_0}{\alpha_0} \Psi. \quad (13)$$

By these transformations, the cubic GS equation becomes

$$u_{,\bar{x}\bar{x}} + u_{,\bar{y}\bar{y}} = -u(1 + u^2). \quad (14)$$

We require $u(\bar{x}, \bar{y})$ to be periodic in the \bar{y} direction, to have the mirror symmetry about the \bar{y} axis, and to become zero at $\bar{x} \rightarrow \infty$. Namely, we look for the solutions which behave solitonlike in the \bar{x} direction.

Let us study the asymptotic behavior of $u(\bar{x}, \bar{y})$ at $\bar{x} \rightarrow \infty$. Since we require that $u(\bar{x}, \bar{y})$ decay in this limit, Eq. (14) is approximated as $u_{,\bar{x}\bar{x}} + u_{,\bar{y}\bar{y}} = -u$. A solution to this equation satisfying the above requirements is

$$u = A \exp\left(-\bar{x}\sqrt{\hat{q}^{-2} - 1}\right) \sin(\hat{q}^{-1}\bar{y}). \quad (15)$$

Here, A and \hat{q} are constants and the value of \hat{q} is limited as $0 \leq \hat{q} \leq 1$. The period in the \bar{y} direction is $\bar{y}_P = 2\pi\hat{q}$. This asymptotic behavior (15) satisfies $u(\bar{x}, 0) = 0$ and

$u_{,\bar{y}}(\bar{x}, \bar{y}_P/4) = 0$, and we assume that these properties are held for all values of \bar{x} . These two relations together with the condition for the mirror symmetry $u_{,\bar{x}}(0, \bar{y}) = 0$ will become the boundary conditions in the numerical calculation. Once the solution satisfying these boundary conditions is generated, the solution in the whole region of (\bar{x}, \bar{y}) is obtained by the relation $u(\bar{x}, \bar{y}) = -u(\bar{x}, -\bar{y}) = u(\bar{x}, \bar{y}_P/4 - \bar{y}) = u(\bar{x}, \bar{y} + \bar{y}_P) = u(-\bar{x}, \bar{y})$.

Note that Eq. (15) is the exact solution of the GS equation (10) in the case $\alpha_0 = 1$ and $\beta_0 = 0$. Therefore, without the cubic term in Eq. (14), the solution diverges at $\bar{x} \rightarrow -\infty$. However, in the case where the cubic term is present, the solution u having the mirror symmetry about the \bar{y} axis can exist because of the nonlinear effect. It will be explicitly shown in Sec. IV.

III. NUMERICAL CALCULATION

In this section, we explain how to calculate the solitonlike solution u of the cubic GS equation (14). The numerical method is explained in Sec. IIIA. In order to establish the existence of the solitonlike solutions, we have to check the numerical errors carefully. This is discussed in Sec. IIIB.

A. Numerical method

In the numerical calculation, it is very convenient to choose the coordinates (X, Y) that are normalized by a quarter of the period in the \bar{y} direction. For this reason, we introduce a parameter

$$q := (\pi/2)\hat{q} \tag{16}$$

and perform the coordinate transformation

$$X := q^{-1}\bar{x}, \quad Y := q^{-1}\bar{y}. \tag{17}$$

In the coordinates (X, Y) , Eq. (14) becomes

$$u_{,XX} + u_{,YY} = -q^2 u(1 + u^2), \tag{18}$$

and the period in the Y direction is $Y_P = 4$. By the symmetries of the solution that we required in Sec. II, it is sufficient to solve in the range $0 \leq X \leq X_{\max}$ and $0 \leq Y \leq 1$.

Here, $X = X_{\max}$ is the outer boundary of the region of numerical calculation, and we choose $X_{\max} = 5$. The error coming from this cutoff value will be estimated in the next subsection.

The boundary conditions are $u = 0$ at $Y = 0$, $u_{,Y} = 0$ at $Y = 1$, and $u_{,X} = 0$ at $X = 0$. At the outer boundary $X = X_{\max}$, we have to impose the condition (15), which is $u = A \exp\left(-X\sqrt{\pi^2/4 - q^2}\right) \sin(\pi/2)Y$ in the (X, Y) coordinates. Because we do not know the value of A before generating the solution of u , we calculate $u_{,X}$ and eliminate A . This leads to the so-called Robin boundary condition

$$u_{,X} = -u\sqrt{\pi^2/4 - q^2}. \quad (19)$$

This formula is used as the boundary condition at $X = X_{\max}$.

In order to solve Eq. (18) numerically, we adopted the second-order finite difference scheme with uniform grids. Since Eq. (18) is an elliptic equation, we have to prepare an initial surface and make it converge to the solution by the method of iteration. However, the solution was found to be unstable against this process. This is in contrast to the case of Ref. [12], where one of us solved a similar equation with no problem. The reason for the difference between the two cases is as follows. In both cases, the equation has the form $\nabla^2 u = -F(u)$. The function $F(u)$ is monotonically decreasing as u grows in the case of [12], while it is a monotonically increasing function in the present case as found from Eq. (18). Let us consider what happens in the latter case. Suppose the initial surface u_0 is slightly larger than the real solution \hat{u} . The program makes the surface approach the solution of the equation $\nabla^2 u = -F(u_0)$. Because $F(u_0) > F(\hat{u})$, the solution of this equation u_1 is further larger than u_0 , i.e. $u_1 > u_0 > \hat{u}$. Therefore, by continuing these processes, the value of u becomes larger and larger and eventually diverges. On the other hand, if u_0 is a little smaller than \hat{u} , the value of u becomes smaller and smaller and collapses to $u = 0$, i.e. the trivial solution. For this reason, the nontrivial solution of Eq. (18) is numerically unstable, and a new idea is needed to obtain it.

Although we could not develop a new code which can automatically generate such numerically unstable solutions, we found a procedure to realize the sufficient convergence of iterations. The point is that for some initial surface u_0 , the surface u approaches the real solution \hat{u} to some extent and then leaves it after that in the process of iteration. In other words, the real solution \hat{u} behaves like an intermediate attractor in this process. Such a behavior typically occurs when u_0 crosses the real solution \hat{u} , i.e. the regions $u_0 > \hat{u}$ and

$u_0 < \hat{u}$ both exist. Using this property, we proceeded as follows. We prepare a good initial surface $u^{(0)}$ and start the computation (the first trial). While the program is running, we observe the convergence parameters

$$\Delta_1 := \frac{\sum |\Delta u_{(I,J)}|}{\sum |u_{(I,J)}|}, \quad \Delta_2 := \max \left| \frac{\Delta u_{(I,J)}}{u_{(I,J)}} \right|, \quad (20)$$

where (I, J) are the label of the grids and $\Delta u_{(I,J)}$ denotes the difference from the finite difference equation. The values of $\Delta_{1,2}$ first decrease and then increase. Just before Δ_1 starts to increase, we write down the surface $u_F^{(0)}$ and stop the program. Then, we prepare the new initial surface $u^{(1)}$ by $u^{(1)} = (1 + \epsilon)u_F^{(0)}$ and run the program again (i.e. the second trial). Choosing ϵ properly, we can make $\Delta_{1,2}$ further smaller although a little experience is required in order to find the effective value of ϵ . We continued these processes of trials until the conditions $\Delta_1 < 10^{-8}$ and $\Delta_2 < 10^{-7}$ are achieved.

B. Error estimates

Using the above technique, we solved the cubic GS equation (18) for $\hat{q} = 0.1$ – 0.9 with 0.1 intervals. In all cases, we adopted the grid numbers (250×50) . Since the solution is numerically unstable, we have to check the numerical error carefully in order to prove that our solution is not a numerical artifact. There are three sources of the numerical errors: the finiteness of X_{\max} , the finiteness of the grid sizes, and the truncation of the convergence process.

The error by the finite X_{\max} value is evaluated by $\delta_1 = [u(X_{\max}, 1)]^2$, since the boundary condition (15) is derived by ignoring the cubic term in Eq. (14). The value of δ_1 is less than 0.02% for $0.1 \leq \hat{q} \leq 0.7$. It becomes larger as \hat{q} is increased and 0.3% for $\hat{q} = 0.9$. This is because the value of u decays very slowly for $\hat{q} \simeq 1$ by the boundary condition (15). We also compared the results of $X_{\max} = 5$ and 10 in the case $\hat{q} = 0.9$. The error estimated in this way is 0.1% .

The error by the finite grid sizes is estimated as 0.03% for all values of \hat{q} by comparing the results of (250×50) and (125×25) grid numbers. This is natural because we used the second-order accuracy scheme and thus the error is expected to have the order of the squared grid size $\sim 0.04\%$.

The error by the truncation of the convergence process is estimated as follows. Suppose u_F

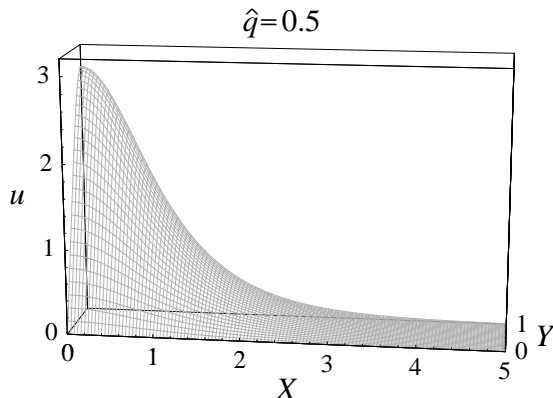


FIG. 1: 3D plot of the generated solution u for $\hat{q} = 0.5$ in the region $0 \leq X \leq 5$ and $0 \leq Y \leq 1$.

is the obtained solution and consider the equation $\nabla^2 u = -q^2 u_F (1 + u_F^2)$. If the convergence is perfect, the solution of this equation is $u = u_F$. Since the convergence process is truncated by the criterion explained above, the actual solution of u is different from u_F , and this difference indicates the error amount. In this way, the error is estimated to be less than 0.03% for all values of \hat{q} .

Therefore, all the numerical errors are small and our results are reliable.

IV. NUMERICAL RESULTS

Now we show the numerical results. Figure 1 shows the 3D plot of the numerical solution of u in the range $0 \leq X \leq 5$ and $0 \leq Y \leq 1$ for $\hat{q} = 0.5$. The solution $u(X, Y)$ takes its maximum value u_{peak} at $(X, Y) = (0, 1)$. Figure 2 shows the behavior of $u(X, 1)$ on the line $Y = 1$ and Fig. 3 shows the behavior of $u(0, Y)$ on the line $X = 0$ (i.e. Y -axis) for $\hat{q} = 0.1$ – 0.9 . The peak value u_{peak} increases as \hat{q} is decreased. This is because the right hand side of Eq. (18) is proportional to q^2 and thus larger value of u is necessary for smaller q in order that the effect of the nonlinear term becomes relevant. From the right plot of Fig. 2, we see that the value of $u(X, 1)$ decays more slowly for larger \hat{q} because of the boundary condition (19).

Figure 4 shows the dependence of the peak value u_{peak} on \hat{q} . From this figure, it is understood that u_{peak} diverges in the limit $\hat{q} \rightarrow 0$. By plotting the relation between $\hat{q}u_{peak}$ and \hat{q} , we found that u_{peak} is approximated by $u_{peak} \simeq 1.72/\hat{q}$ for small \hat{q} . The solution of u becomes $u \equiv 0$ in the limit $\hat{q} \rightarrow 1$, because u depends only on Y in this limit by the boundary

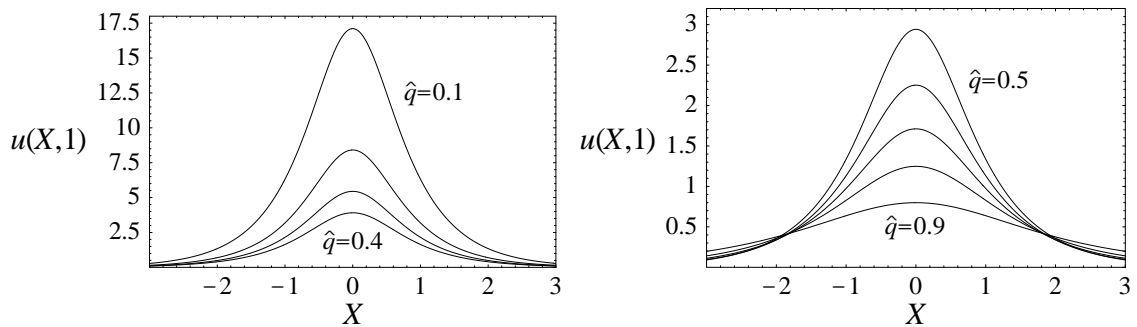


FIG. 2: The behavior of $u(X, 1)$ on the line $Y = 1$ for $\hat{q} = 0.1-0.4$ (left) and $\hat{q} = 0.5-0.9$ (right).

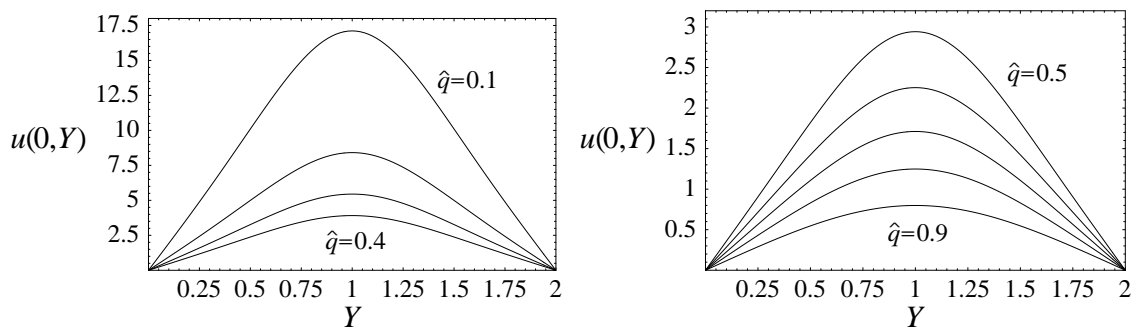


FIG. 3: The behavior of $u(0, Y)$ on the Y -axis for $\hat{q} = 0.1-0.4$ (left) and $\hat{q} = 0.5-0.9$ (right).

condition (19) while we are solving the sequence for which $u = 0$ at $X = \infty$. By plotting the values of u_{peak}^2 as a function of $1 - \hat{q}$, we found that the formula $u_{peak} \simeq 2.27\sqrt{1 - \hat{q}}$ approximately holds in the neighborhood of $\hat{q} = 1$.

We summarize the general properties that do not depend on specific forms of f and g . From Eqs. (12) and (17), the coordinates (X, Y) and (x, y) are related as $X = \alpha_0 \hat{q}^{-1} x$ and

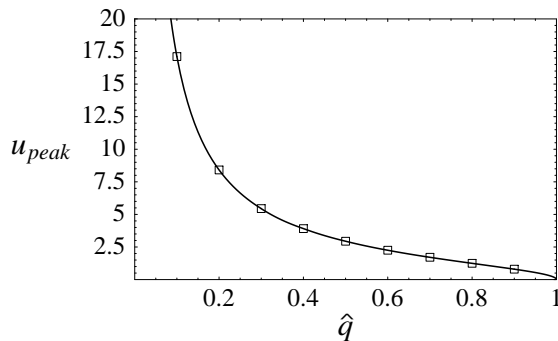


FIG. 4: The dependence of the peak value u_{peak} on \hat{q} . The numerical data is shown by squares (\square). u_{peak} behaves as $u_{peak} \propto \hat{q}^{-1}$ and $\sqrt{1 - \hat{q}}$ in the neighborhood of $\hat{q} = 0$ and 1 , respectively.

$Y = \alpha_0 q^{-1} y$. In the (x, y) coordinates, the period of Ψ in the y direction is

$$y_P = \frac{4q}{\alpha_0}. \quad (21)$$

By the dimensional analysis, $f(\Psi)$ and $g(\Psi)$ are found to be expressed as

$$f(\Psi) = \frac{\alpha_0^2}{\beta_0} \hat{f}(u), \quad g(\Psi) = \frac{\alpha_0^4}{\beta_0^2} \hat{g}(u). \quad (22)$$

Here, by Eq. (11), $\hat{f}(u)$ and $\hat{g}(u)$ are related as

$$\hat{f}^2 + 2\hat{g} = u^2 + \frac{u^4}{2} + \hat{C}, \quad (23)$$

where \hat{C} is a non-negative constant. Calculating the magnetic field (3) and the electric current (4) using Eqs. (8), (13) and (10), we obtain

$$\mathbf{B} = \frac{\alpha_0^2}{\beta_0} \left[\frac{1}{q} (-u_{,Y} \mathbf{e}_x + u_{,X} \mathbf{e}_y) + \hat{f}(u) \mathbf{e}_z \right], \quad (24)$$

$$\mathbf{J} = -\frac{\alpha_0^3}{\beta_0} \left[\frac{\hat{f}_{,u}}{q} (-u_{,Y} \mathbf{e}_x + u_{,X} \mathbf{e}_y) + u(1 + u^2) \mathbf{e}_z \right]. \quad (25)$$

From these formulas, the meanings of the parameters q , α_0 , and β_0 are understood. Since the inside of the parenthesis of Eq. (24) depends only on u and q (for a fixed form of \hat{f}), the direction of the magnetic field at a given position (X, Y) is determined once the value of q is specified. This means that the shape similarity of the field lines is preserved when α_0 and β_0 are varied. Furthermore, nondimensional quantities such as the beta ratio $2p/B^2$ are independent of α_0 and β_0 . Therefore, q is the parameter that determines all nondimensional properties of the system. For a fixed q , the value of α_0 determines the characteristic scale of the system through Eq. (21). After fixing q and α_0 , the magnitude of \mathbf{B} is determined by specifying β_0 . Hence β_0 is (say) the field strength parameter.

From x and y components of Eqs. (24) and (25), the magnetic field lines and the electric currents are confined on the contour surfaces of u . Figure 5 shows the contours of u on the (X, Y) -plane for $\hat{q} = 0.5$. The directions of the magnetic fields are also shown. The magnetic fields are clockwise in the region $u > 0$ and counter-clockwise in the region $u < 0$. From Eq. (25), it is seen that $J_z < 0$ in the region $u > 0$ and $J_z > 0$ in the region $u < 0$. This relation between the directions of (B_x, B_y) and the sign of J_z is consistent with Ampere's law.

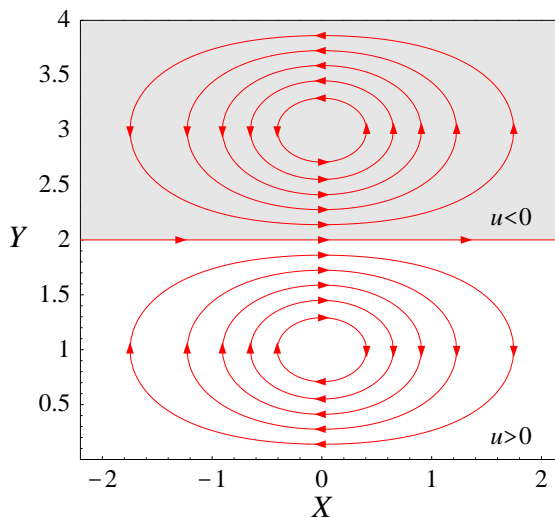


FIG. 5: The contours of $|u| = 0.0$ – 2.5 (with 0.5 intervals) for $\hat{q} = 0.5$ on the (X, Y) -plane. The arrows indicate the directions of magnetic field lines. They are clockwise in the region $u > 0$ and counter-clockwise in the region $u < 0$.

The z component of the magnetic field is specified by the function $\hat{f}(u)$. Changing $\hat{f}(u)$ affects (J_x, J_y) through Ampere's law. If $\hat{f}(0) = 0$ and $\hat{f}(u)$ is a monotonic function in each region of $u > 0$ and $u < 0$, a simple relation exists between the sign of B_z and the directions of (J_x, J_y) . Let us consider the region $u > 0$. If $\hat{f}(u)$ is a monotonically increasing function, we have $\hat{f} > 0$ and $\hat{f}_{,u} > 0$. This indicates that $B_z > 0$ and the electric currents are counter-clockwise. On the other hand, if $\hat{f}(u)$ is a monotonically decreasing function, we have $\hat{f} < 0$ and $\hat{f}_{,u} < 0$, which means that $B_z < 0$ and the electric currents are clockwise. The same relation is obtained also for $u < 0$.

V. SUMMARY AND DISCUSSION

In this paper, we studied the solitonlike solutions of magnetostatic equilibria by numerically solving the cubic GS equation. Although the solutions were unstable against the numerical iteration, we found the procedure to realize the sufficient convergence and obtained the highly accurate solutions. The generated solutions are solitonlike in the x direction, periodic in the y direction and symmetric in the z direction. Our result proves the existence of the solitonlike solution that was questioned in recent years [2, 3, 4, 5, 6].

The solitonlike solution obtained in this paper behaves as an even function on a $y = \text{const.}$

line and has one extreme at the center. It is interesting to examine the existence of another solution that behaves as an odd function on a $y = \text{const.}$ line and has an extreme in each region of $x > 0$ and $x < 0$. Such a (say) 2-solitonlike solution could be expected by the following discussion. Denoting the obtained solitonlike solution by $\Psi^{(1)}(x, y)$, the function

$$\Psi^{(2)}(x, y) = \Psi^{(1)}(x - d/2, y) - \Psi^{(1)}(x + d/2, y) \quad (26)$$

also approximately satisfies the GS equation (10) for sufficiently large d , since $\Psi^{(1)}(x)$ decays exponentially for large $|x|$. Therefore, one might expect the existence of 2-solitonlike solutions also for finite values of d . However, it is possible to show that no 2-solitonlike solution exists under the boundary condition $\Psi(0, y) = 0$ for any f and g satisfying $f(0)f'(0) + g'(0) = 0$. To show this, we multiply $\Psi_{,x}$ to the GS equation (9) as

$$\Psi_{,xx}\Psi_{,x} + \Psi_{,yy}\Psi_{,x} = -(ff' + g')\Psi_{,x}, \quad (27)$$

and integrate this equation over the region $0 \leq x \leq \infty$ and $0 \leq y \leq y_P$. Assuming the exponential decay of Ψ at $x \gg 1$, the integrals of the second term on the left hand side and the right hand side vanish, and we have

$$\int_0^{y_P} \Psi_{,x}^2(0, y) dy = 0, \quad (28)$$

and therefore $\Psi_{,x}(0, y) = 0$. Then, the GS equation (9) indicates that all derivatives of Ψ with respect to x vanish on the symmetry axis (assuming Ψ to be analytic). Hence $\Psi = 0$ is the only solution. Physically, this means that when two or more solitons coexist, they interact each other and cannot be in equilibrium.

It is interesting to discuss the stability of the solitonlike solution obtained in this paper. The system is expected to be unstable, since the magnetic islands are periodically located in the y direction and interactions between them are present. The most important factor for such interactions is the directions of the electric currents of the islands. If the currents of the islands are parallel (i.e., J_z has the same sign), the islands attract each other and coalesce into larger islands. Such instability is known as the coalescence instability [13, 14]. On the other hand, if the currents of the neighboring islands are anti-parallel (i.e., J_z has an alternating sign), their interaction is repulsive and they tend to repel each other in the x direction as a result of small disturbance. Since J_z has an alternating sign in our system as seen from Eq. (25), the repulsive instability is expected. In fact, both instabilities were

confirmed by the recent numerical work on the dynamics of magnetic islands with parallel and anti-parallel currents [6].

Although the plane-symmetric solitonlike solution in this paper could be of use in the contexts of the astrophysics or the solar physics, it would be more interesting to apply our method to the axisymmetric case. In the observations of active galactic nuclei (AGN), the astrophysical jets are often found to have knotty structures that suggest the presence of magnetic multiple islands [7]. Several models of the knotty jets have been proposed, and one of the possible directions is to model the knotty jets as magnetostatic equilibria [2, 4, 6, 8, 9]. Although these studies do not give the mechanism for the formation of the knotty jets, such models are expected to explain the long lifetime of collimation and knotty structure simultaneously. Namely, the knotty jets can maintain their shapes because they are in equilibrium in the comoving frame, and the time scale of the instabilities gives the lifetime of the knotty structure. The authors of [6] studied the growth of instabilities of plane-symmetric solitonlike configurations by performing numerical simulations. Assuming that the plane-symmetric solitonlike systems well approximate the axisymmetric ones, they compared the results with the observations of the knotty jet of the radio galaxy 3C 303 [15, 16, 17]. Their conclusion is that the numerical simulation gives good agreement with the actual observations. Here, it should be pointed out that the assumption in that paper is not obvious and has to be justified. For this reason, the extension to the axisymmetric cases is necessary in order to examine if the solitonlike solutions can really model the astrophysical knotty jets. An axisymmetric quasiperiodic magnetostatic solution of the linear GS equation was proposed as the astrophysical jet model [9]. The numerical method in this paper enables us to generalize the study of [9] to the case of the nonlinear axisymmetric GS equation and thus to obtain further large class of astrophysical jet models as magnetostatic equilibria. The present work is the first step toward this direction, and we are planning to generalize our result to the axisymmetric case. It would be also interesting to further explore the solitonlike solutions in the helically symmetric cases.

Acknowledgments

HY thanks the Killam Trust for financial support.

- [1] D. Biskamp, *Nonlinear Magnetohydrodynamics* (Cambridge University Press, Cambridge, 1993).
- [2] G. Lapenta, Phys. Rev. Lett. **90**, 135005 (2003) [arXiv:astro-ph/0303448].
- [3] G. N. Throumoulopoulos, K. Hizanidis, and H. Tasso, Phys. Rev. Lett. **92**, 249501 (2004).
- [4] G. Lapenta, Phys. Rev. Lett. **92**, 249502 (2004).
- [5] P. K. Shukla, L. Stenflo and O. A. Pokhotelov, Phys. Scripta T**116**, 135 (2005).
- [6] G. Lapenta and P. P. Kronberg, Astrophys. J. **625**, 37 (2005).
- [7] A. H. Bridle, D. H. Hough, C. J. Lonsdale, J. O. Burns and R. A. Laing, Astron. J. **108**, 766 (1994).
- [8] A. Königel and A. R. Choudhuri, Astrophys. J. **289**, 137 (1985).
- [9] O. I. Bogoyavlenskij, Phys. Rev. Lett. **84**, 1914 (2000).
- [10] V. I. Petviashvili, O. A. Pokhotelov, and N. V. Chudin, Sov. Phys. JETP **55**, 1056 (1982).
- [11] V. I. Petviashvili, O. A. Pokhotelov, and L. Stenflo, Sov. J. Plasma Phys. **12**, 545 (1986).
- [12] H. Yoshino, T. Shiromizu and M. Shibata, Phys. Rev. D **74**, 124022 (2006) [arXiv:gr-qc/0610110].
- [13] J. M. Finn and P. K. Kau, Phys. Fluids **20**, 72 (1977).
- [14] P. L. Pritchett and C. C. Wu, Phys. Fluids **22**, 2140 (1979).
- [15] P. P. Kronberg, Astrophys. J. **203**, L47 (1976).
- [16] J. P. Leahy and R. A. Perley, Astron. J. **102**, 537 (1991).
- [17] J. Kataoka, P. Edwards, M. Georganopoulos, F. Takahara and S. Wagner, Astron. Astrophys. **399**, 91 (2003).